International Journal of Heat and Mass Transfer 177 (2021) 121528

Contents lists available at ScienceDirect

International Journal of Heat and Mass Transfer

journal homepage: www.elsevier.com/locate/hmt

Transport behavior of pressure-driven gas flow in a nanochannel and the variation of thermal accommodation coefficient

Sooraj K. Prabha[a,*], C.P.A. Gafoor[a], Sarith P. Sathian[b]

[a] Department of Mechanical Engineering, Vidya Academy of Science and Technology, Thrissur 680501, India
[b] Department of Applied Mechanics, Indian Institute of Technology Madras, Chennai 600036, India

ARTICLE INFO

Article history:
Received 12 February 2021
Revised 11 May 2021
Accepted 22 May 2021

Keywords:
Transport behavior
Pressure-driven gas flow
Rarefied gas flow
Thermal accommodation coefficient
Molecular dynamics
Nanochannel

ABSTRACT

A three-dimensional molecular dynamics simulation of a rarefied gas flow confined between two parallel solid walls has been carried out to study the gas transport behavior in nanoscale pressure-driven flows. To simulate the effects of pressure-driven flows in nanoscale systems; a reservoir is created at the beginning of the channel. A force, in the form of *gravity*, is applied to every gas molecule occupying a specific region in the reservoir thereby facilitating to establish a streamwise inhomogeneous flow in a finite length nanochannel. Further, the model is tested for its structural stability and steady-state characteristics. The flow characteristics are evaluated at various bins (A, B, C, and D) along the length of the channel. The presence of a pressure drop established along the length of the channel results in a significant variation of flow properties in the channel. The characteristics of the system are further studied using the spatial distribution of flow properties. To investigate the streamwise variation, thermal accommodation coefficients (TACs) at various sections of the channel are calculated. The results indicate that the TACs vary along the length. Further, the effect of pressure drop on TACs is also analysed. The effect of confinement is also studied with velocity autocorrelation function (VACF) and mean squared displacement (MSD). The effect of confinement is evident in the fluid region away from the wall too.

1. Introduction

Gas flows through micro/nanoscale channels is an important consideration in the design of MEMS/NEMS sensors and devices, miniaturised heat exchangers for electronics cooling, gas filtration/separation technologies, extraction of shale gas, etc. The flow through micro/nanochannels has been studied extensively in the recent past to characterize the gas flow at smaller dimensions. As the size of the channel decreases, the characteristic dimension of the system is of the order to the mean free path of the gas. Consequently, the flow characteristics deviate severely from the macroscale continuum behavior of the gas flows [1,2].

Knudsen number ($Kn = \lambda/H$) is used to categorize the flow regimes based on the characteristic dimension H and the mean free path λ of the system. The gas flows at nanoscale mainly fall into the slip and the transition regime [1]. In such gas flow regimes, the collisions between gas and wall dominate over intermolecular gas collisions. This leads to the breakdown of the continuum assumption in these flow regimes and it demands a molecular level analysis[1].

The analysis of microscopic kinetics of the gas and surface molecules will give a better insight into the heat transfer phenomenon in nanoscale gas flows [3–5]. The fluid-solid interface characteristics such as velocity slip and temperature jump is crucial in small scale channel flows [6]. The information regarding the thermal accommodation coefficient (TAC) is inevitable for calculating heat transfer at the interface and the resulting flow properties. The idea of TAC was first introduced by Maxwell and later clearly defined by Knudsen in his work on the kinetic theory of gases. The TAC is the measure of energy interactions between the gas and the solid surface when the gas-particle undergoes a collision with the surface. TAC is defined as,

$$\alpha_E = \left\langle \frac{E_I - E_O}{E_I - E_T} \right\rangle, \tag{1}$$

where E is the energy of the gas atom that interacts with the surface. The subscript I denotes incident molecules, O denotes reflecting molecules, and T denotes the thermal wall condition. The angled bracket $\langle .. \rangle$ denotes the ensemble average.

TAC in nanoscale gas transport problems has been studied using experimental and computational methods. Molecular beam experiments have been widely employed to measure energy accommodation coefficients [7,8]. Recently, an optical method is demonstrated

* Corresponding author.
E-mail address: sooraj.kp@vidyaacademy.ac.in (S.K. Prabha).

https://doi.org/10.1016/j.ijheatmasstransfer.2021.121528
0017-9310/

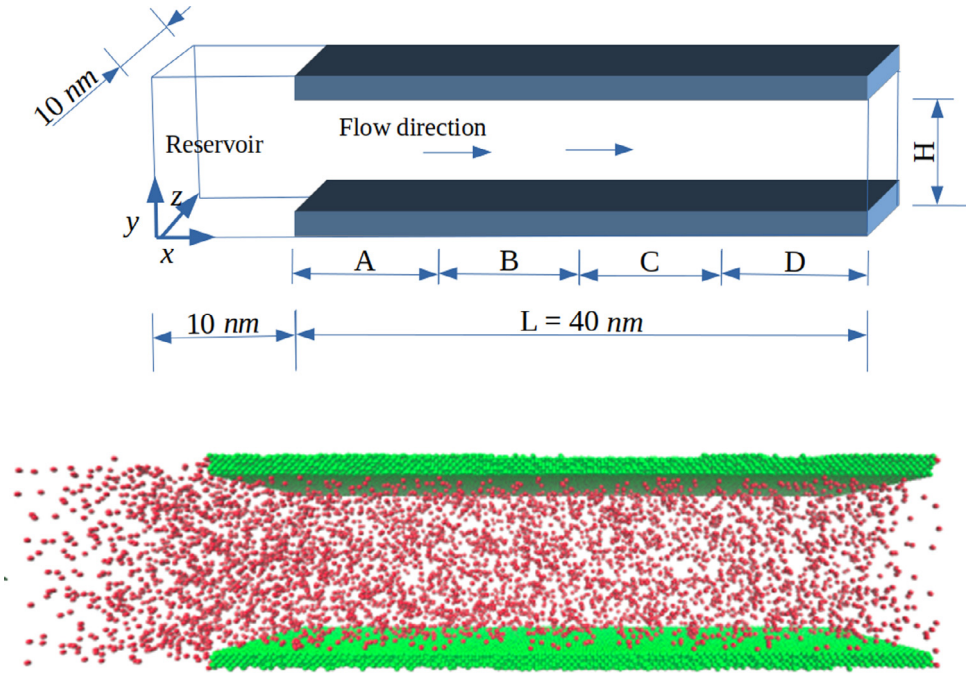

Fig. 1. The schematic representation of the simulation domain (The schematic is not drawn to scale). The left extreme portion is the reservoir and the rest of the domain is the channel section. Positive *x*-direction is taken as the flow direction. The channel length is divided into different bins (A,B,C, and D) for the convenience of analysis. The picture of actual simulation domain in MD is shown below the schematic representation.

to measure the TAC relating to the variation of thermal conductivity [9]. Attempt to evaluate TAC from interactions of a binary gas mixture by measuring the conductive heat flux is also reported [10].

Numerical techniques, which model the heat transfer in micro/nanosystems, employ TAC as the phenomenological parameter to analyze flow characteristics such as temperature jump at the boundary [11,12]. For instance, Lattice Boltzmann method (LBM) [13] and the direct simulation Monte Carlo (DSMC) method [14,15] are widely used numerical techniques for analyzing micro/nanoflow characteristics. These techniques employ various scattering models such as the Cercignani-Lampis (CL) to model the gas-surface interactions [11,16]. The accuracy of these models predominately relies upon accommodation coefficients (AC). The CL model uses two ACs, while some other scattering models use even more number of ACs when the complexity increases [17].

The advancement in computer hardware helped the research community to employ atomistic modeling of micro/ nanoscale systems using molecular dynamics (MD) simulations. In MD simulations, properties are calculated by averaging the properties of the individual atoms or molecules and their interactions. Therefore, it makes MD a suitable choice to investigate flow properties such as TAC. The momentum and energy accommodation coefficients for a stagnant monatomic gas confined between two parallel plates have been reported by considering the individual gas collision data generated from MD [18,19]. The accommodation coefficients of the Poiseullie flow through nanochannels have also been studied from the individual collision data, and the effect of Knudsen number on ACs have been explored [20,21]. Further, the dependence of molar proportions on TAC for a binary gas mixture is also reported [22]. Parametric studies on TAC reveal that it is influenced by many factors such as gas/solid materials, surface roughness, and wall temperature [21,23–27]. The MD studies also reveal that the ACs are dependent on interaction parameters (interaction strength, molecular mass, the molecular size of the gas) [5,28]. However, the variation of TACs along the length of the channel and its influence on a pressure-driven flow are yet to be investigated.

The mean-squared displacement (MSD) and velocity autocorrelation function (VACF) are useful tools that can be used with the data obtained from MD to analyze the transport mechanism at molecular scale [29,30]. MD simulations have enabled the self-diffusion properties analyzed for a liquid-gas or liquid-solid interface[31]. Einstein's equation can be effectively used to determine the surface diffusion coefficients of gas molecules on a solid surface[32]. Knudsen diffusion is highly relevant where the mean free path is significantly larger than the characteristic dimension [33,34]. The confinement of gas in a nanochannel is found to have an influence on the MSD and VACF characteristics significantly [30,35]. Moreover, in nanochannel flows, the flow conditions can vary from high pressure to low pressure. Subsequently, the transport mechanisms also change in accordance with the pressure changes and the resulting rarefaction levels [36].

In most of the studies employing MD, infinite length channel with a zero pressure drop in the streamwise direction was considered. In such studies it is not possible to analyse the streamwise variations of the flow characteristics as in a pressure-driven flow. On the otherhand, modeling and simulation of pressure-driven gas flows are more challenging, especially when the channel length is larger when compared to the characteristic dimension. (For example, due consideration should be given to the structural integrity of the simulation model, the presence of unbalanced forces, relatively higher kinetic energy of the gas molecules, the higher pressure gradients, etc.). Further, the flows through nanochannels exhibit a streamwise inhomogeneity, and rarefaction levels of the stream will increase along the downstream. The *gravity/force* driven methods are widely used due to its simplicity [20,21,36], but it is not recommended for the study of pressure drop in long channels. In the dual control volume method (popularly known as DCV-GCMD), Monte Carlo (MC) techniques are used to maintain the number of particles inside the reservoirs and, the movements of molecules are obtained by employing the MD [37]. Reflecting Particle Membrane (RPM) is another method used to model the pressure-driven flows in nanoscale conduits [38–40]. A modified form of external gravity-driven flow to induce a pressure gradient in the channel is also

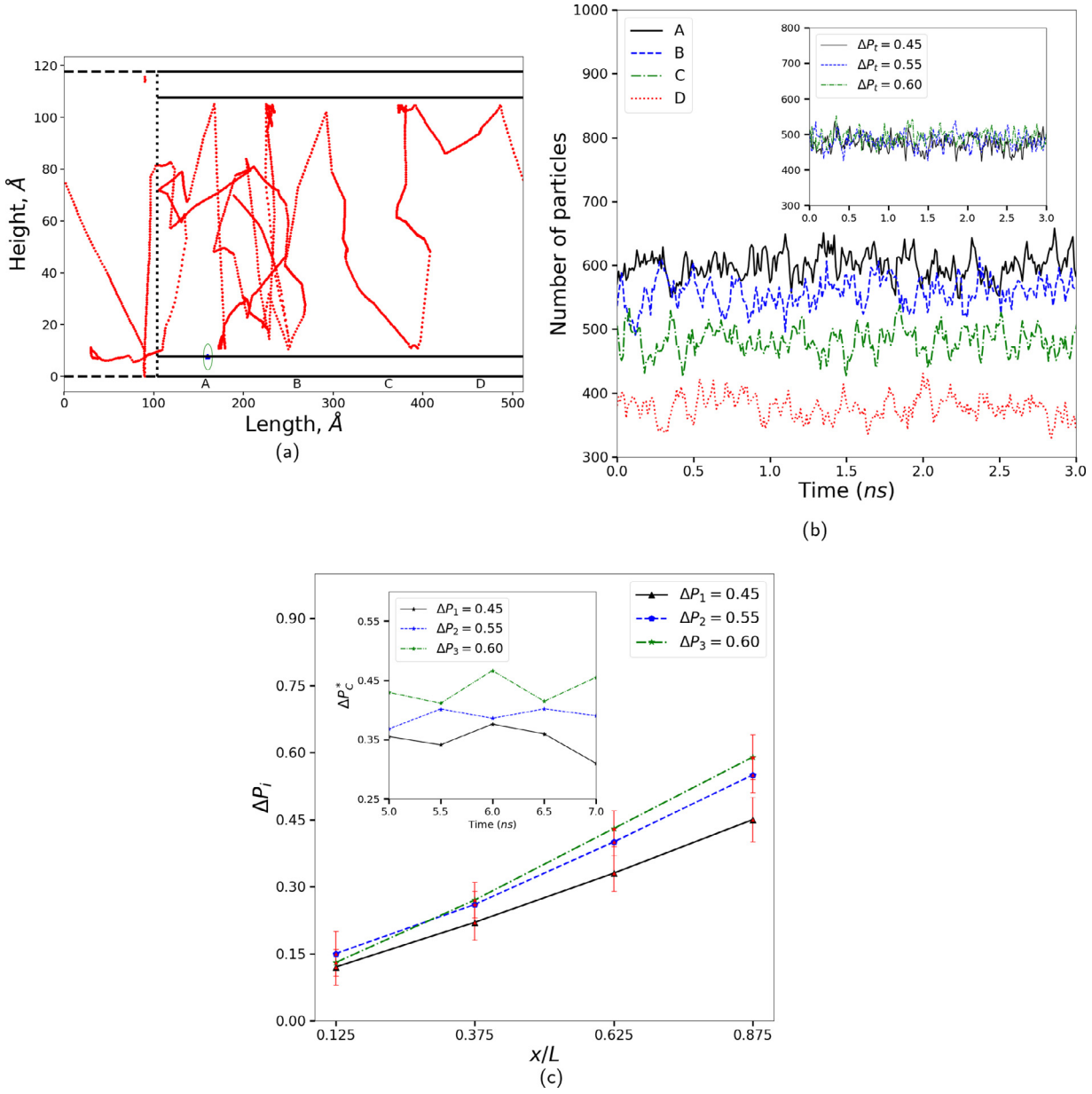

Fig. 2. (a) A single gas molecule (red points) is tracked for a finite number of time-steps. The horizontal lines (black) represent the solid wall. The horizontal dotted lines represent the boundary of the reservoir. The effect of confinement is visible in the trajectory of the randomly selected gas molecule. (b) The number of gas atoms with respect to time at various locations of the channel is shown. This is for a pressure drop of 0.55. The inset shows the number of gas atoms in bin C, and it is stable for all three values of pressure drop. (c) Normalized values of pressure drop at different length sections is shown. The pressure drop in each bin is normalized with the respective reservoir pressure, P_0. A linear relationship between ΔP and normalized length is observed. Inset shows the pressure drop in bin C for different total pressure drops. The pressure drop is found stable throughout the simulation period.

used for this purpose [41,42]. In this approach, an external gravity is applied only to a small portion of the reservoir, and the channel portion is completely kept undisturbed. In the present study, we employ this method to generate a pressure drop along the channel.

The main objective of this study is to understand the effect of pressure drop and the varying rarefaction in the channel on the gas transport and the thermal accommodation coefficients along the length. In this work, we have used the molecular dynamics method to study the flow characteristics of pressure-driven flow. MD simulations have been performed using LAMMPS package [43]. A detailed analysis of the stability of the simulation model and the variation of relevant properties have been discussed in detail. The key feature of this study is the calculation of thermal accommodation coefficients by tracking the individual collisions and its variation along the length of the channel. Further, the influence of pressure drop on thermal accommodation coefficients has been discussed in detail. The microscale flow characteristics are further explored with MSD and VACF. It is observed that the thermal accommodation properties are varying with pressure drop, and consequently, the properties associated with it are also affected.

This paper is organized as follows. The computational details of the system are described in section II; section III presents results and discussion. Section IV represents the conclusion. The results are further subdivided into different parts. The structural and steady-state characteristics of the system are discussed in the first part of the results and discussion. The variation of relevant physical properties is given in the next section. The accommodation coefficients are discussed next, and finally, the MSD and VACF characteristics are discussed.

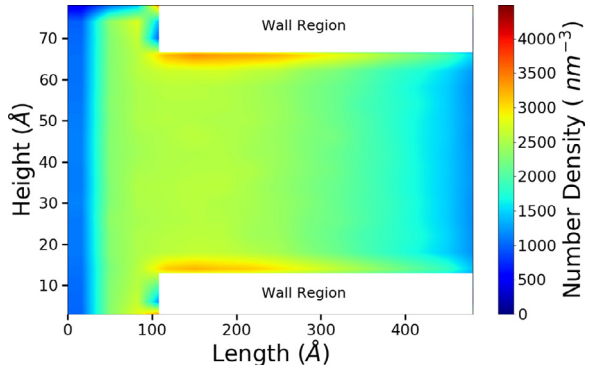

Fig. 3. The variation of number density is shown in a 2D plane (*xy*). The density near the wall region shows a higher value when compared to the bulk flow region. A decrease in density along the length can also be observed.

2. Details of simulation model

A three-dimensional Poiseuille flow of a rarefied gas (Argon) between two parallel walls (Platinum) is studied. LAMMPS is used for modeling and simulation of the system considered [43]. The wall atoms are arranged in the FCC structure with a lattice constant of 0.392 nm. The gas atoms are initially configured randomly in between the parallel walls. The average Knudsen number in all the bins for every test case is calculated, and its range is found between 0.20 to 0.60. This indicates that the flow is in the transition regime. The dimensions of the simulation domain are chosen to be 50 x (6 + 2*W*) x 10 *nm*, where *W* is the thickness of the wall (Fig. 1 [44]). The flow direction is in the positive *x*-direction, and the characteristic dimension *H* is in the *y*-direction.

The interactions between the molecules in the system are modeled using Lennard-Jones (LJ) pairwise potential field, which is defined as,

$$U_{ij}(r_{ij}) = 4\varepsilon_{ij}\left[\left(\frac{\sigma_{ij}}{r_{ij}}\right)^{12} - \left(\frac{\sigma_{ij}}{r_{ij}}\right)^{6}\right], \tag{2}$$

where r_{ij}, ε_{ij} and σ_{ij} is the distance between two particles, interaction strength, and LJ length parameter, respectively. The values of the LJ parameters are given in Table 1 [18,22]. To initialize the simulation, the gas atoms are assigned with an initial velocity corresponding to the bulk temperature. A truncated LJ potential field is employed with cutoff distance σ_c equal to 2.5 σ. The selection of σ_c depends on the potential field strength ε and the rarefaction level of the flow. The MD movements of the particles are calculated by integrating the equation of motion using a Velocity-Verlet algorithm. The selection of time step for the integration in MD is a pivotal parameter which influences the solution accuracy, stability of the model and the computational cost. The time step chosen in the present study is 1 *fs* [45]. The temperature of the wall is maintained at 400 *K* using a Berendsen thermostat [46].

Table 1
LJ Parameters used for the simulation.

Interactions	ε (*eV*)	σ (*nm*)	σ_c (*nm*)
Ar-Ar	0.01029	0.341	0.6175
Ar-Pt	0.00682	0.294	0.8513
Pt-Pt	0.32501	0.247	0.7343

In the present model, the total length of the simulation domain is divided into two regions: i) a reservoir region and ii) a channel region of length L = 40 *nm*. To establish a pressure gradient along the channel, an external *gravity* is applied only to the gas atoms at the entry of the reservoir region. The gas particles present in the remaining part of the reservoir and the channel region is not subjected to any external force. Hence, it can be asserted that the flow in the channel is completely kept undisturbed by the external force, and the flow develops as a result of the pressure drop developed in the channel. This arrangement satisfies the requirement for the condition of a streamwise inhomogeneous flow.

3. Results and discussion

To facilitate the analysis, the channel length L is subdivided into four bins viz. A, B, C, and D (Fig. 1). This helps to analyze the characteristics at various locations of the channel as the flow proceeds downstream. The system is equilibrated for 4 *ns* before collecting the MD data for calculating flow properties. The system is tested for its structural and thermodynamic stability.

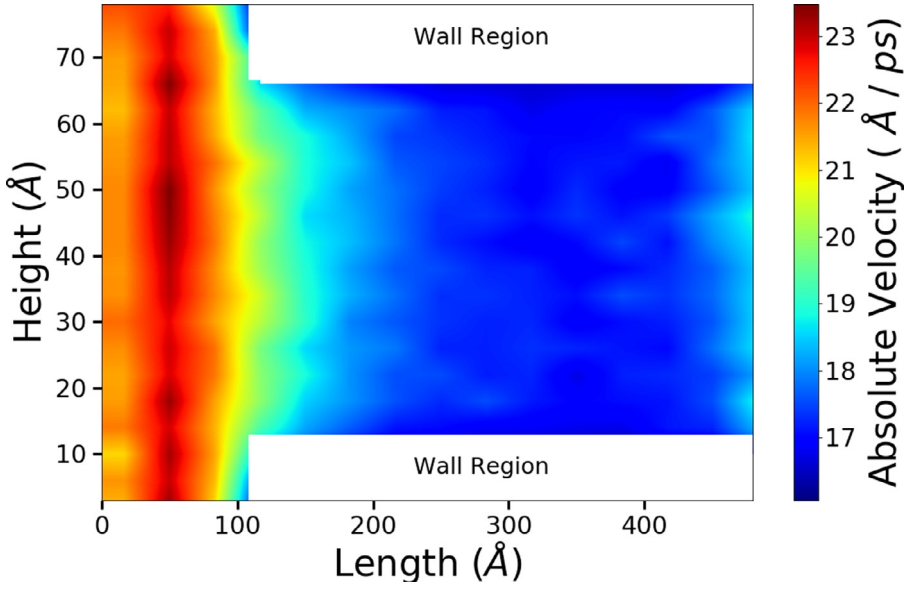

Fig. 4. The variation of absolute velocity is portrayed in a 2D plane (*xy*). The velocities have a higher value in the upstream. A *gravity* is provided to molecules in a specific region in the middle of the reservoir, which is visible.

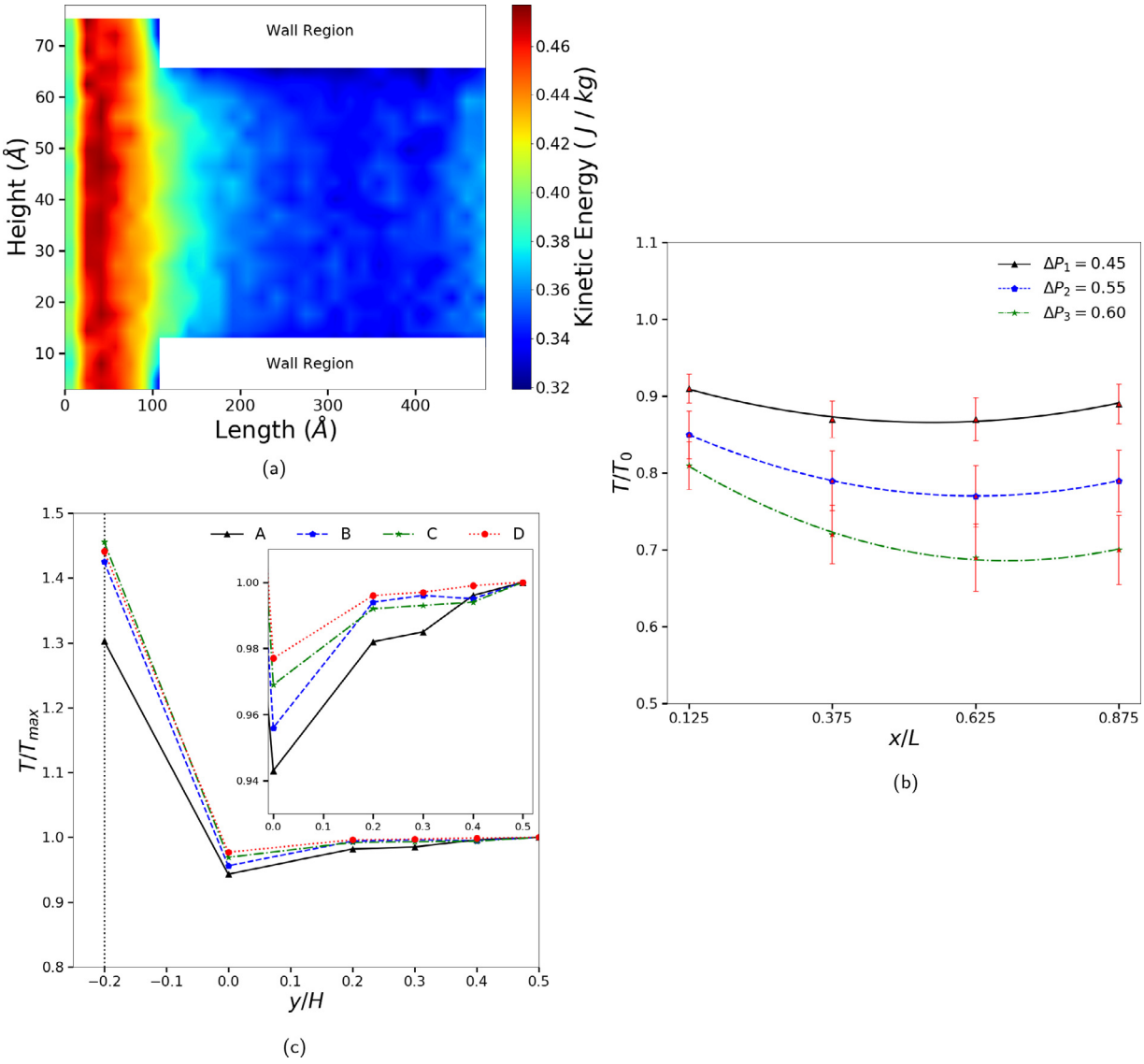

Fig. 5. The variation of temperature in the channel is shown. (a) The specific kinetic energy (KE$\propto$ T) variation in a 2D plane (xy). A nonhomogeneous distribution along the length is visible from the figure. Also, a near-wall discontinuity is observed. (b) The variation of temperature against length of the channel is shown. The temperature is normalised with respective reservoir temperature T_0. (c) Temperature profile across the channel in different sections for half of the channel is shown. Temperature is normalised with the maximum temperature in the respective bin. Temperature discontinuity at the wall is also visible.

3.1. Stability and steady-state

While simulating the flow of gas in relatively longer channels for a longer duration of time, the structural stability of the simulation domain is an important requirement. To this end, we have followed certain procedures to build a stable simulation model.

3.1.1. Trajectory

Following the method described in our previous study [42], the structural integrity of the system is studied by considering the trajectory of a single molecule over a simulation period from both fluid and solid (Fig. 2 (a)). From the trajectory of the fluid molecule, the effect of confinement is visible, and the solid wall is capable of maintaining structural integrity. A, B, C, and D indicate the positions of the bins. The system must reach a steady-state before it is being considered to analyze the flow characteristics.

3.1.2. Steady-state

To examine this, the average number of particles in all the four bins is plotted against time (Fig 2 (b)). From the figure, it can be observed that the number of particles in each bin remains constant (with acceptable statistical fluctuations) throughout the simulation period. Further, the average number of particles in a bin (bin C) is plotted against the time for all the three pressure drops (Fig. 2 (b) inset). Likewise, in the previous case, the central tendency of the number of particles in bin C for all three pressure drops is also constant. Therefore, it can be concluded that the system has attained a steady-state for all the values of pressure drop considered for the study. The temperature at various locations in the simulation domain is also tracked to verify the steady-state conditions.

3.1.3. Pressure drop

The pressure drop at various sections along the length is plotted in Fig. 2 (c). The pressure drop at each bin is normalized with the reservoir pressure and calculated as $\Delta P_i = (P_0 - P_i)/P_0$, where P_i is the pressure at the respective bins of the channel, and P_0 is the pressure at the reservoir. Further, to investigate the effect of pressure drop on flow properties, three cases with different val-

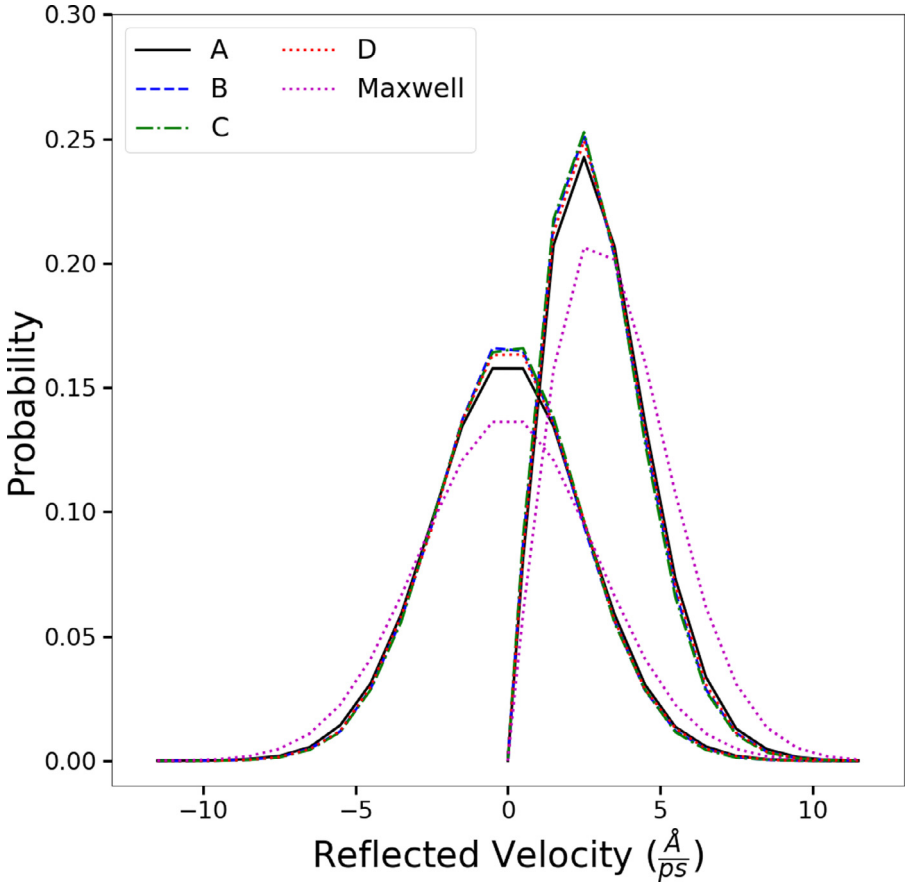

Fig. 6. The probability distributions of the reflected velocity/speed for gas molecules at different bins. The Maxwell's velocity distribution for the wall temperature is compared with the reflected distributions.

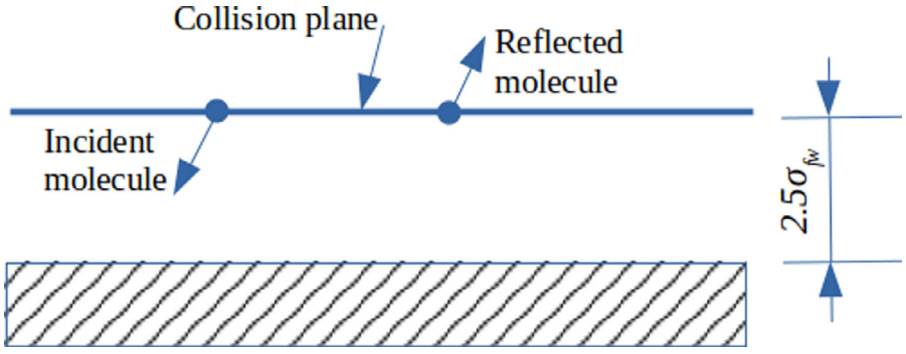

Fig. 7. The schematic representation of the collision tracking mechanism is shown here (The schematic is not drawn to scale). The respective components are logged when the molecule crosses the collision tracking plane.

ues of total pressure drop along the channel are considered. These cases are identified as $\Delta P_1 = 0.45 \pm 0.06$, $\Delta P_2 = 0.55 \pm 0.06$ and $\Delta P_3 = 0.60 \pm 0.06$ throughout the discussions (Fig. 2 (c)). It can be seen that pressure drop is varying linearly with the normalized length.

It is visible from Fig. 2 (c) that the flow gets rarefied in a finite length nanochannel as the flow proceeds downstream. Consequently, a higher slope in the curve is observed with ΔP_3. The inset shows the pressure drop in bin C of the channel for all the three pressure drops (ΔP_1, ΔP_2, and ΔP_3) for a finite duration of the simulation. The average pressure drop is constant throughout the simulation time. These results indicate the thermodynamic stability of the model.

3.2. Spatial distributions

Gas flows through nanoscale systems possess peculiar characteristics such as density accumulation near the solid boundary, velocity slip, temperature jump, variation of density in the flow direction, etc. This necessitates a more involved analysis of such flow systems. In this study, the gas flow characteristics are verified and analyzed through the spatial distribution of crucial properties.

3.2.1. Density

The distribution of density indicates the non-homogeneous nature of nanoscale flows in a pressure-driven flow. The near-wall accumulation of gas molecules is visible in the density distribution (Fig. 3). From the color pattern, it can be observed that there is density accumulation near the wall [when compared to the bulk

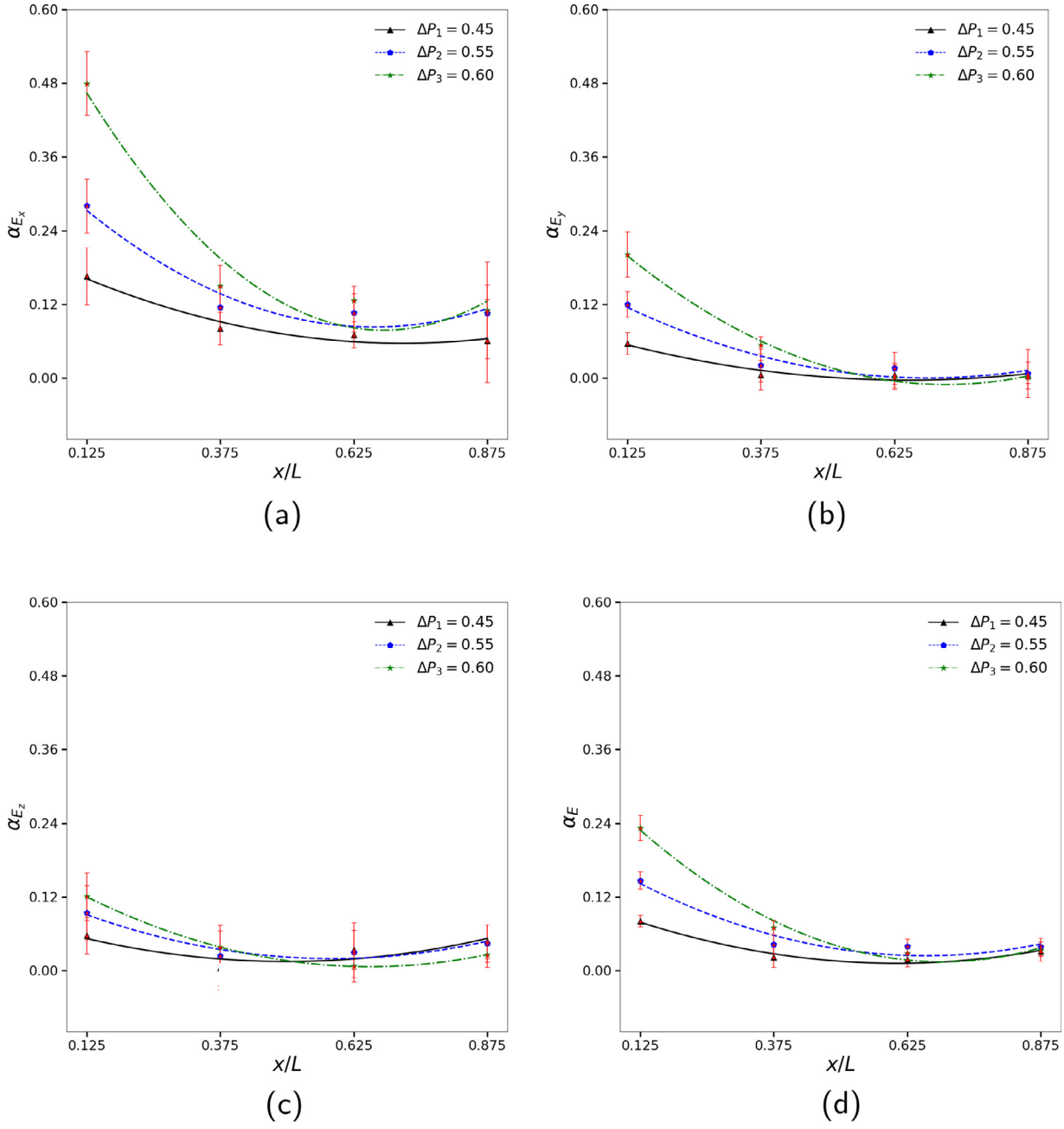

Fig. 8. Thermal accommodation coefficients at different sections are shown. Three cases of pressure drops in the channel are considered. The sub-figures a, b, c represents TAC components in x, y, z directions respectively. The total thermal accommodation coefficient is also shown in sub-figure d.

flow region] throughout the channel. This is one of the important characteristics of the rarefied flows. A decrease in density is seen downstream as the flow gets more rarefied with respect to the pressure drop. The effect of the periodic boundary is also visible in the channel exit region.

3.2.2. Velocity

The spatial variation of the absolute velocity over the simulation domain is shown in Fig. 4. Each point in the 2D space gives a qualitative and quantitative assessment of velocity and, consequently, momentum. From the color pattern, it can be observed that at a given cross-section of the flow, the velocity is maximum at the middle portion and is minimum at the boundary/wall region, but not zero. This clearly indicates the validity of the slip condition. The velocity is very low in the wall region that is exposed to the reservoir. The *gravity* is made effective in a specific region in the reservoir, which is also visible from the color pattern. A detailed study of velocity profiles and momentum accommodation has already been reported in our previous study [42].

3.2.3. Temperature

The temperature of an ideal monatomic gas is proportional to its kinetic energy. Therefore, the spatial variation of KE is similar to the spatial variation of temperature. To visualize the same, the specific KE (KE$\propto$ T) is plotted as a 2D heatmap over the simulation domain (Fig. 5 (a)). From the figure, it can be observed that there is a non-homogeneous distribution at the beginning of the channel and nonhomogeneity decreases as the flow proceed downstream. The effect due to periodic boundary conditions is also visible in the exit region.

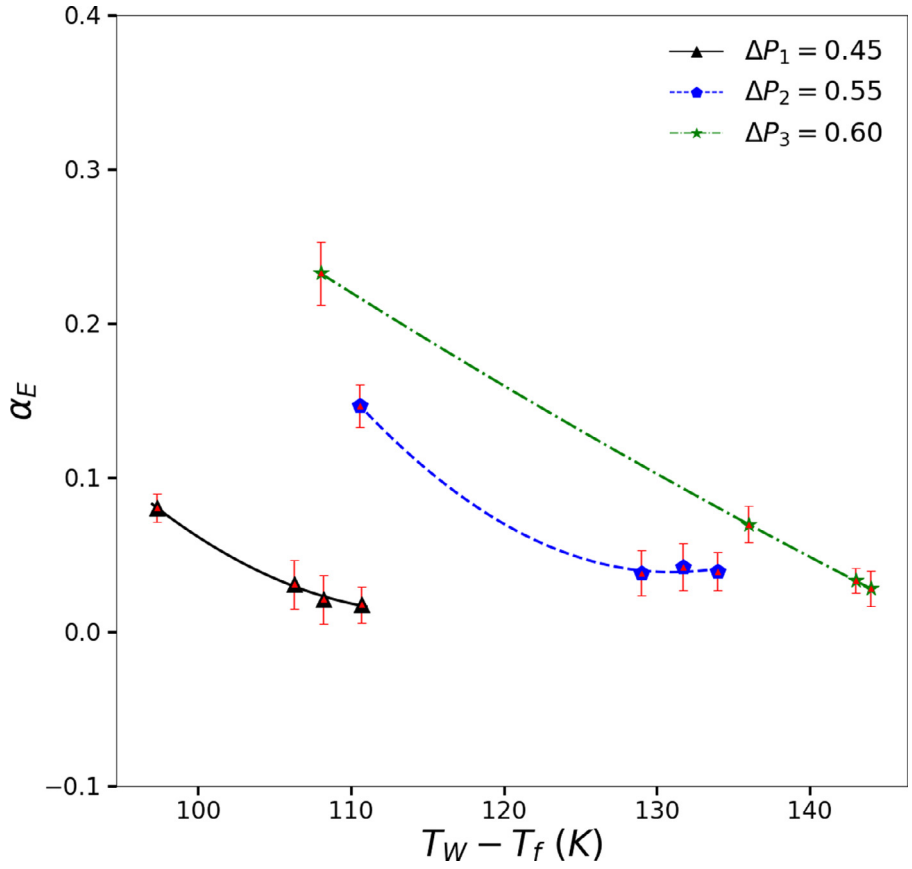

Fig. 9. TAC is plotted against temperature jump ($T_w - T_f$)for three different pressure drops. Temperature jump between the wall and gas molecules near the wall influences the TAC.

When the channel is subjected to a pressure drop, the expansion of the gas will occur along the flow direction. Consequently, the temperature is expected to drop in the channel along the length. To examine this characteristic of pressure-driven flows, the average temperature at each bin is plotted, as shown in Fig. 5 (b). The rate of temperature drop is observed to increase as the pressure drop increases in the early stages of the flow. Please note that the temperature drop is insignificant further down the stream.

Further, to examine the discontinuity (also called temperature jump) in the gas-surface interface, the temperature profile across the flow direction y is calculated, and the temperature is normalized with the maximum temperature $T_{\max}$ at each bin (Fig. 5 (c)). The left extreme points represent the wall temperature that is normalized with the corresponding $T_{\max}$. This discontinuity in the temperature profile near the wall is a well-known behavior of the rarefied flows. Further, it can be noted that the discontinuity becomes larger as the flow proceeds downstream. In downstream, as the flow gets rarefied, there is a subsequent reduction in the average number of gas-wall collisions, which in turn influences the discontinuity. In addition to this, the temperature profile is showing deviation from the basic parabolic nature across the channel. This variation of properties near the wall region will have an effect on dynamics of the reflected molecules from the surface.

3.2.4. Velocity/speed distributions

The velocity/speed distributions of gas molecules emanated from the wall at different locations of the channel have been illustrated in Fig. 6. As the solid wall is maintained at a constant temperature, the reflected distributions at different locations would have taken the same shape on full accommodation. However, from the figure, it is observed that the reflected distributions are different from each other. Further, the distributions are compared with Maxwell's distribution for the wall temperature, and it can be presumed that partial accommodation exists at the nanochannel surface. The signs of partial accommodation are evident from the temperature profiles too. Hence, the thermal accommodation properties of the flow are investigated in detail in the following sections.

3.3. Thermal accommodation coefficients

The Thermal Accommodation Coefficient (TAC), also called the energy accommodation coefficient, is considered as an important parameter to characterize the gas-wall interaction and the heat transfer at the interface. The calculation of thermal accommodation coefficients (Eqn. 1) requires the individual collision data of gas molecules. To this end, the incoming and the outgoing velocities of gas atoms after every collision with the wall are recorded [18,47]. To facilitate this, a virtual plane is positioned near the wall at a distance of 2.5 σ_{fw}, where σ_{fw} is the LJ length parameter for Ar-Pt interactions (Fig. 7). To find the accommodation properties in a bin, the collisions data in each bin are collected separately.

3.3.1. Thermal accommodation: components

Both the tangential and normal components of TAC are depicted in Fig. 8 that are calculated from the corresponding energy components of the molecules. The TACs in tangential direction decreases along the length of the channel. This can be evident from the figure (Fig. 8(a) and (c)). This can be attributed to the decrease in the pressure, the gas-wall collision frequency, and increase in the rarefaction levels, etc. A similar trend can be found in the normal

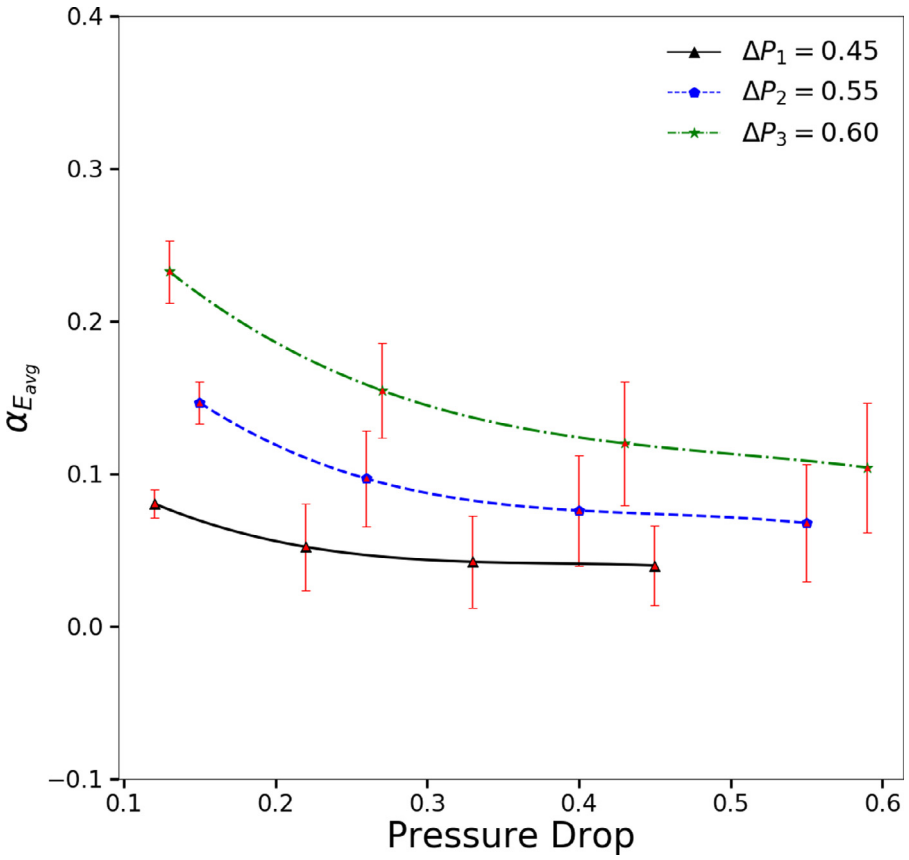

Fig. 10. The average values of TACs for the respective pressure drops are plotted. The average TACs show a linear variation with the smaller pressure drops. As the pressure drop increases, the variation in average TAC value is minimal.

component of TAC (Fig. 8 (b)). Nevertheless, a slight increase in TACs towards the downstream is observed in all three directions. As the difference in temperature of the gas and the wall molecules increases in the downstream, this behavior can be expected. Further, TAC corresponding to the total energy component is also plotted in Fig. 8(d).

3.3.2. Temperature jump

The temperature jump and accommodation property influence each other. In other words, partial accommodation can cause temperature jump and vice versa. The near-wall temperature can be obtained by averaging the properties in the bin adjacent to the wall. As the wall is maintained at a constant temperature, the difference between the temperature of the wall (T_w) and the temperature of the fluid adjacent to the wall (T_f) gives the amount of discontinuity present at the interface. From Fig. 9, it is observed that the near-wall temperature is one of the influencing factors of TAC. The TAC increases with a decrease in the discontinuity ($T_w - T_f$).

3.3.3. Pressure drop

From these results, it is understood that the TAC decreases down the channel. However, it is interesting to see its variation with pressure drop, which is one of the measurable characteristics of the nanoscale system. To this end, the average values of TACs for a finite length is plotted against the respective pressure drop. (For example, the total pressure drop in bin B is found as $(P_0 - P_B)/P_0$), and the average value of TAC is calculated by considering the collisions up to including bin B). As seen in Fig. 10, TAC decreases with an increase in the pressure drop. When the average TAC is calculated for a longer section, the error bars are showing higher values. The variation of TAC is almost linear for the lower value of pressure drop.

3.4. MSD and VACF

The transport coefficients are related to the statistical averages of the individual molecular motion parameters. The transport properties under the confinement can be significantly affected by the choice of the wall models [48]. This has motivated us to study the microscopic transport behavior with the solid wall modeling. To study the effect of confinement in the fluid region away from the wall, MSD and VACF of the fluid in the channel is studied. To this end, the fluid molecules in this region region (i.e., the region in between the collision tracking planes on both sides) are analyzed, and the results are as follows.

3.4.1. MSD

The mean-squared displacement (MSD) will enable the study of the diffusion behavior of the flow inside the channel. As the flow is subjected to various pressure drops at different points in the channel, it is expected to have distinct diffusion characteristics.

The MSD is calculated as,

$$MSD = \langle [r_i(t) - r_i(0)]^2 \rangle, \tag{3}$$

where $r_i(t)$ is the position of the i^{th} particle at time step t and $r_i(0)$ is the reference position of the i^{th} particle. The symbol $\langle . \rangle$ denotes the ensemble average.

As the flow proceeds, the pressure and number density are found to be reduced; consequently, the flow rarefaction increases.

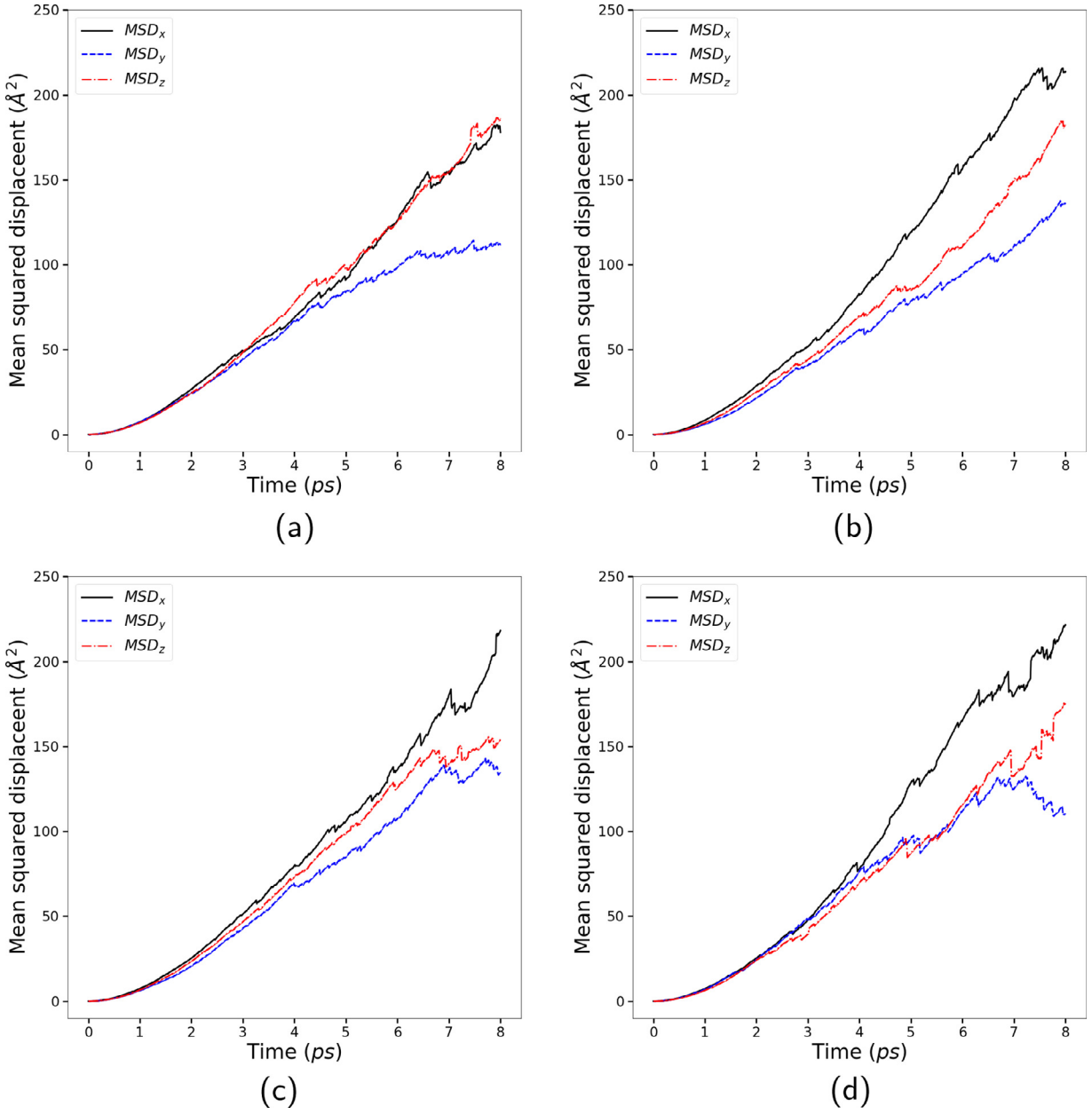

Fig. 11. Mean squared displacement in three directions at various locations (bins) of the channel((a) A (b) B (c) C (d) D). The directions x and z are parallel to the solid surface, and y is perpendicular to the solid surface. All the components represents the behavior in the region (where surface potentials are absent). The short-time MSD of perpendicular direction shows the effect of confinement. The effect due to pressure drop is visible in all cases.

This has multiple effects on the MSD in different directions. Therefore, it is interesting to study the effect of these parameters on the MSD.

The MSD is plotted against time in Fig. 11, and it represents the flow behavior at different sections of the channel. At the beginning of the channel, the curves for x and z directions are similar in nature as they represent the parallel components. Indeed, the x component deviates from z as time progresses because the drift component of motion starts to surface. Please note that the normal component has a lower value in all the bins, which is attributed to the confinement effect. As MSD is for the bulk flow region, it is devoid of the effect due to direct interaction with the wall. However, the secondary collisions of reflected molecules from the wall have an influence on the fluid away from the wall. This behavior is visible throughout the channel length. Further downstream, the slope of the MSD is increasing, which can be attributed to the higher rarefaction levels in the downstream of the channel.

3.4.2. VACF

The VACF reflects the characteristics of the motion of molecules in gases. The VACF is determined as,

$$VACF_i = \frac{\langle [v_i(t) * v_i(0)] \rangle}{\langle [v_i(0) * v_i(0)] \rangle}, \tag{4}$$

where $v_i(t)$ is the i_{th} molecule at time t. The velocity at the initial condition is represented with $v_i(0)$. The VACF is normalized with the initial velocity.

For the initial period, all three VACFs show an exponentially decreasing trend (Fig. 12). This is similar to the behavior of the bulk fluid. A monotonic decay trend is expected for unconfined fluid [35]. As the flow progresses, the parallel and perpendicular components show distinct behavior. The VACF becomes oscillatory, which is typical to the confined fluids. Apart from that, the following observation can be made from the figures. Firstly, the best-fit curves (not shown in the figure) in the y-direction approaches the hori-

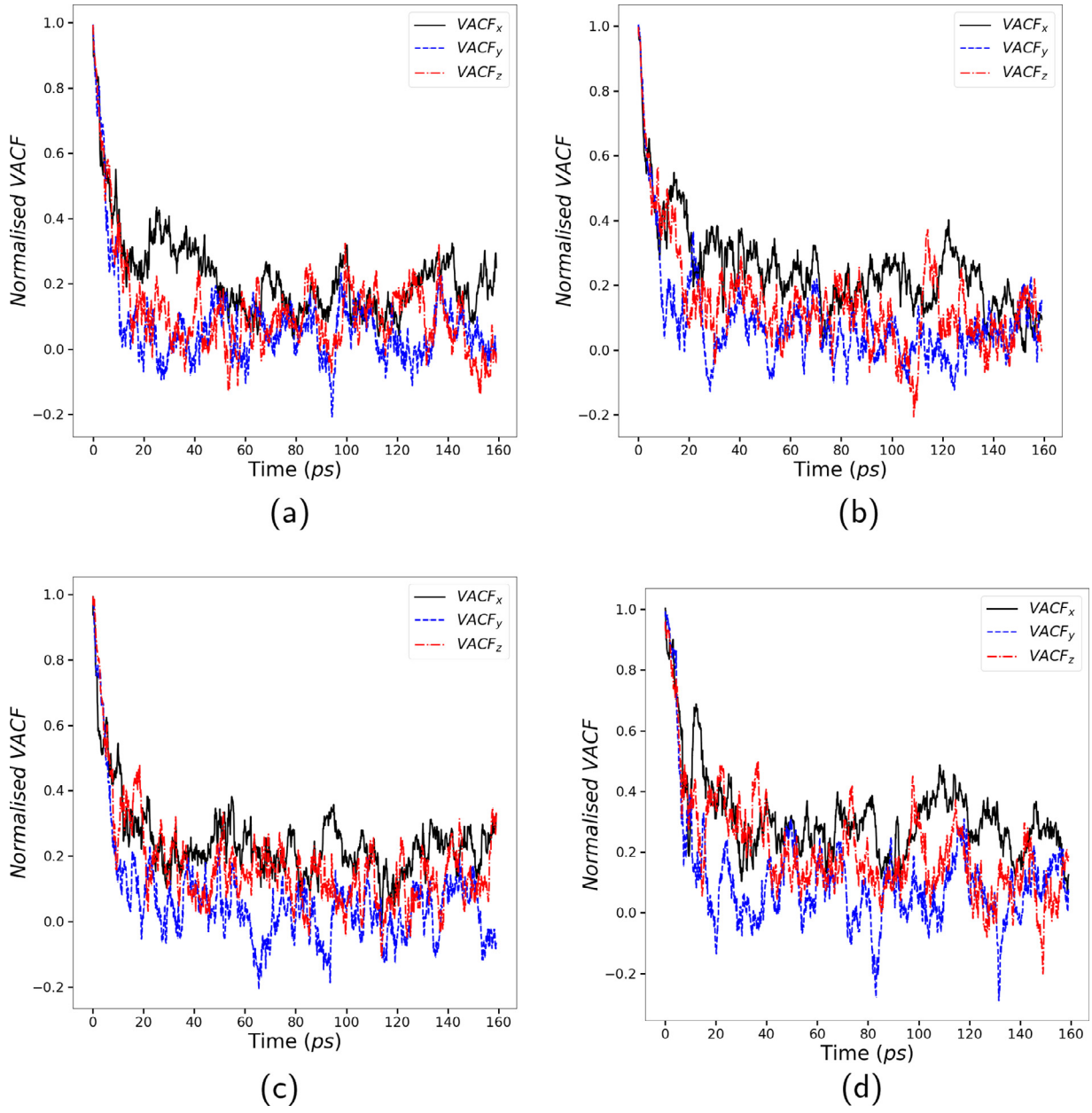

Fig. 12. Normalised velocity auto-correlation function in three directions at various bin of the channel ((a) A (b) B (c) C (d) D). The directions x and z are parallel to the solid surface, and y is perpendicular to the solid surface. All the VACF components are normalised with the initial values. All the components represents the behavior in the fluid region away from the wall. The VACF in the perpendicular direction shows the effect of confinement.

zontal axis at a faster rate in all the bins. This effect is attributed to the presence of boundary and the collisions with the reflected molecules from the surface. Secondly, as the flow proceeds, all the VACF components approaches the horizontal axis at a slower rate, which is attributed to the rarefaction effect. When the rarefaction increases, the mean-time between collisions in the bulk region will increase.

4. Conclusion

In this study, extensive molecular dynamics simulations have been performed to investigate the characteristics of nanoscale pressure-driven flows through a channel. A streamwise inhomogeneous flow in a finite length channel has been realized by introducing a reservoir at the beginning of the channel. A detailed study on the effect of the total pressure drop in the channel has been done. The stability of the simulation model has been investigated first and, subsequently, the spatial variation of the relevant properties. The flow properties density, velocity, temperature, etc., are found to vary along the flow direction as well as across the flow direction. A higher rarefaction is observed in the downstream as the flow proceeds. A temperature discontinuity and change in its profile is also observed near the wall region where the size effects are predominant. This behavior is a typical characteristic of rarefied flows in nanoscale conduits.

The thermal accommodation coefficient is determined at respective bins to investigate the gas-surface interactions further. The individual collisions of molecules are tracked to find the thermal accommodation properties. This has been performed by defining a virtual plane near the wall. The TAC, calculated at different length sections, are evaluated to elucidate the effect of pressure drop in the channel. The average TAC for a particular length is found to

vary with the pressure drop. From the results, it can be concluded that the variation in TAC is distinct at different locations along the length. Hence, it is suggested that the analytical and numerical models which employ TAC, in their boundary conditions, should consider its variation with length.

The microscopic transport behavior has been studied with the MSD and VACF. The MSD was studied for a short time of 8 *ps* for which the drift motion is negligibly small. However, the drift effect in the flow direction and the effect due to confinement in the perpendicular direction of flow were visible in the MSD of the fluid away from the wall. The effect due to rarefaction down the channel was also visible. A similar distinction can also be made from the VACF components too. The VACF components show a monotonic decay in the beginning, and as time progresses, it approaches the horizontal axis at a faster rate when the density is relatively high and vice versa. Therefore, it can be concluded that the rarefied gas flow properties are also strongly influenced by the nanoconfinement.

Author Agreement Statement

We, the authors of this work hereby declare that this manuscript is original, has not been published before and is not currently being considered for publication elsewhere. We confirm that the manuscript has been read and approved by all named authors and that there are no other persons who satisfied the criteria for authorship but are not listed. We further confirm that the order of authors listed in the manuscript has been approved by all of us.

We understand that the Corresponding Author is the sole contact for the Editorial process.

He/she is responsible for communicating with the other authors about progress, submissions of revisions and final approval of proofs.

Declaration of Competing Interest

We, the authors of this paper hereby declare the following

All authors have participated in (a) conception and design, or analysis and interpretation of the data; (b) drafting the article or revising it critically for important intellectual content; and (c) approval of the final version.

This manuscript has not been submitted to, nor is under review at, another journal or other publishing venue.

The authors have no affiliation with any organization with a direct or indirect financial interest in the subject matter discussed in the manuscript.

Acknowlgedgments

The authors are grateful for the research grant by SERB, Department of Science and Technology, Government of India for this work, vide sanction No. ECR/2017/000326/ES (Ver-1).

References

[1] G. Karniadakis, A. Beskok, N. Aluru, Microflows and nanoflows: fundamentals and simulation, 29, Springer Science & Business Media, 2006.
[2] A. Agrawal, A comprehensive review on gas flow in microchannels, Int J Micronano Scale Transp (2012).
[3] S. Saxena, R. Afshar, Thermal accommodation coefficient of gases on controlled solid surfaces: argon-tungsten system, Int J Thermophys 6 (2) (1985) 143–163.
[4] A. Giri, P.E. Hopkins, Analytical model for thermal boundary conductance and equilibrium thermal accommodation coefficient at solid/gas interfaces, J Chem Phys 144 (8) (2016) 084705.
[5] H. Sha, R. Faller, G. Tetiker, P. Woytowitz, Molecular simulation study of aluminum–noble gas interfacial thermal accommodation coefficients, AlChE J. 64 (1) (2018) 338–345.
[6] R. Wang, J. Du, Z. Zhu, Effects of wall slip and nanoparticles' thermophoresis on the convective heat transfer enhancement of nanofluid in a microchannel, J. Therm. Sci. Technol. 11 (1) (2016) JTST00017.
[7] S.C. Saxena, R.K. Joshi, Thermal accommodation and adsorption coefficients of Gases, 1989.
[8] N. Selden, N. Gimelshein, S. Gimelshein, A. Ketsdever, Analysis of accommodation coefficients of noble gases on aluminum surface with an experimental/computational method, Physics of Fluids 21 (7) (2009) 073101.
[9] D. Ganta, E. Dale, J. Rezac, A. Rosenberger, Optical method for measuring thermal accommodation coefficients using a whispering-gallery microresonator, J Chem Phys 135 (8) (2011) 084313.
[10] H. Yamaguchi, J. Hosoi, Y. Matsuda, T. Niimi, Measurement of conductive heat transfer through rarefied binary gas mixtures, Vacuum 160 (2019) 164–170.
[11] J. Sun, Z.-X. Li, Molecular dynamics simulations of energy accommodation coefficients for gas flows in nano-channels, Mol Simul 35 (3) (2009) 228–233.
[12] B.-Y. Cao, M. Chen, Z.-Y. Guo, Temperature dependence of the tangential momentum accommodation coefficient for gases, Appl Phys Lett 86 (9) (2005) 091905.
[13] S. Chen, G.D. Doolen, Lattice boltzmann method for fluid flows, Annu Rev Fluid Mech 30 (1) (1998) 329–364.
[14] G.A. Bird, J. Brady, Molecular gas dynamics and the direct simulation of gas flows, 42, Clarendon press Oxford, 1994.
[15] M. Wang, Z. Li, Simulations for gas flows in microgeometries using the direct simulation monte carlo method, Int. J. Heat Fluid Flow 25 (6) (2004) 975–985.
[16] H. Struchtrup, Maxwell boundary condition and velocity dependent accommodation coefficient, Physics of Fluids 25 (11) (2013) 112001.
[17] N. Andric, D.W. Meyer, P. Jenny, Data-based modeling of gas-surface interaction in rarefied gas flow simulations, Physics of Fluids 31 (6) (2019) 067109.
[18] P. Spijker, A.J. Markvoort, S.V. Nedea, P.A. Hilbers, Computation of accommodation coefficients and the use of velocity correlation profiles in molecular dynamics simulations, Physical Review E 81 (1) (2010) 011203, doi:10.1103/PhysRevE.81.011203.
[19] S.K. Prabha, S.P. Sathian, Computational study of thermal dependence of accommodation coefficients in a nano-channel and the prediction of velocity profiles, Computers & fluids 68 (2012) 47–53.
[20] S.K. Prabha, S.P. Sathian, Molecular-dynamics study of poiseuille flow in a nanochannel and calculation of energy and momentum accommodation coefficients, Physical Review E 85 (4) (2012) 041201.
[21] K.K. Kammara, R. Kumar, Development of empirical relationships for surface accommodation coefficients through investigation of nano-poiseuille flows using molecular dynamics method, Microfluid Nanofluidics 24 (9) (2020) 1–14.
[22] S.K. Prabha, S.P. Sathian, Determination of accommodation coefficients of a gas mixture in a nanochannel with molecular dynamics, Microfluid Nanofluidics 13 (6) (2012) 883–890.
[23] K. Yamamoto, H. Takeuchi, T. Hyakutake, Characteristics of reflected gas molecules at a solid surface, Physics of Fluids 18 (4) (2006) 046103.
[24] H. Ambaye, J. Manson, Calculations of accommodation coefficients for diatomic molecular gases, Physical Review E 73 (3) (2006) 031202.
[25] J. Blömer, A. Beylich, Molecular dynamics simulation of energy accommodation of internal and translational degrees of freedom at gas–surface interfaces, Surf Sci 423 (1) (1999) 127–133.
[26] W.W. Lim, G.J. Suaning, D.R. McKenzie, A simulation of gas flow: the dependence of the tangential momentum accommodation coefficient on molecular mass, Physics of Fluids 28 (9) (2016) 097101.
[27] Z. Liang, P. Keblinski, Parametric studies of the thermal and momentum accommodation of monoatomic and diatomic gases on solid surfaces, Int J Heat Mass Transf 78 (2014) 161–169.
[28] H. Yamaguchi, Y. Matsuda, T. Niimi, Molecular-dynamics study on characteristics of energy and tangential momentum accommodation coefficients, Physical Review E 96 (1) (2017) 013116.
[29] H. Wang, L. Chen, Z. Qu, Y. Yin, Q. Kang, B. Yu, W.-Q. Tao, Modeling of multi--scale transport phenomena in shale gas productiona critical review, Appl Energy 262 (2020) 114575.
[30] V.Y. Rudyak, A. Belkin, D.A. Ivanov, V.V. Egorov, The simulation of transport processes using the method of molecular dynamics. self-diffusion coefficient, High Temp. 46 (1) (2008) 30–39.
[31] P. Liu, E. Harder, B. Berne, On the calculation of diffusion coefficients in confined fluids and interfaces with an application to the liquid- vapor interface of water, The Journal of Physical Chemistry B 108 (21) (2004) 6595–6602.
[32] C. Sun, B. Bai, Gas diffusion on graphene surfaces, PCCP 19 (5) (2017) 3894–3902, doi:10.1039/C6CP06267A.
[33] Z. Li, L. Hong, On the knudsen transport of gases in nanochannels, J Chem Phys 127 (7) (2007) 074706.
[34] S. Gruener, P. Huber, Knudsen diffusion in silicon nanochannels, Phys. Rev. Lett. 100 (6) (2008) 064502.
[35] K. Ghosh, C. Krishnamurthy, Molecular dynamics of partially confined lennard-jones gases: velocity autocorrelation function, mean squared displacement, and collective excitations, Physical Review E 98 (5) (2018) 052115.
[36] H. Yu, J. Fan, J. Chen, Y. Zhu, H. Wu, Pressure-dependent transport characteristic of methane gas in slit nanopores, Int J Heat Mass Transf 123 (2018) 657–667.
[37] A.P. Thompson, D.M. Ford, G.S. Heffelfinger, Direct molecular simulation of gradient-driven diffusion, J Chem Phys 109 (15) (1998) 6406–6414.
[38] J. Li, D. Liao, S. Yip, Coupling continuum to molecular-dynamics simulation: reflecting particle method and the field estimator, Physical Review E 57 (6) (1998) 7259.
[39] F. Bao, Y. Huang, Y. Zhang, J. Lin, Investigation of pressure-driven gas flows in nanoscale channels using molecular dynamics simulation, Microfluid Nanofluidics 18 (5–6) (2015) 1075–1084.

[40] F. Bao, Y. Huang, L. Qiu, J. Lin, Applicability of molecular dynamics method to the pressure-driven gas flow in finite length nano-scale slit pores, Mol Phys 113 (6) (2015) 561–569.
[41] M. Kazemi, A. Takbiri-Borujeni, Non-equilibrium molecular dynamics simulation of gas flow in organic nanochannels, J Nat Gas Sci Eng 33 (2016) 1087–1094.
[42] S.K. Prabha, A.G. C. P., S.P. Sathian, Variation of momentum accommodation coefficients with pressure drop in a nanochannel, Phys. Rev. E 102 (2020) 023303, doi:10.1103/PhysRevE.102.023303.
[43] S. Plimpton, Fast parallel algorithms for short-range molecular dynamics, J Comput Phys 117 (1) (1995) 1–19.
[44] W. Humphrey, A. Dalke, K. Schulten, Vmd: visual molecular dynamics, J Mol Graph 14 (1) (1996) 33–38.
[45] R. Wang, S. Qian, Z. Zhang, Investigation of the aggregation morphology of nanoparticle on the thermal conductivity of nanofluid by molecular dynamics simulations, Int J Heat Mass Transf 127 (2018) 1138–1146.
[46] H.J. Berendsen, J.v. Postma, W.F. van Gunsteren, A. DiNola, J. Haak, Molecular dynamics with coupling to an external bath, J Chem Phys 81 (8) (1984) 3684–3690.
[47] S.K. Prabha, S.P. Sathian, Velocity distribution and velocity correlation of mixture of gases in a nanochannel, Int. J. Therm. Sci. 81 (2014) 52–58.
[48] Q. Cai, M.J. Biggs, N.A. Seaton, Effect of pore wall model on prediction of diffusion coefficients for graphitic slit pores, PCCP 10 (18) (2008) 2519–2527.